NMR spin-lattice relaxation and ionic conductivity in lithium thioborogermanate fast-ion-conducting glasses

Benjamin Meyer,[1,*] Ferdinando Borsa,[2,3] David M. Martin,[1] and Steve W. Martin[1,†]
[1]*Department of Materials Science & Engineering, Iowa State University, Ames, Iowa 50011, USA*
[2]*Department of Physics and Astronomy and Ames Laboratory, Iowa State University, Ames, Iowa 50011, USA*
[3]*Dipartimento di Fisica "A. Volta" e Unità INFM di Pavia, Università di Pavia, 27100 Pavia, Italy*
(Received 20 November 2003; revised manuscript received 26 January 2005; published 3 October 2005)

^{7}Li nuclear spin-lattice relaxation (NSLR) and ionic conductivity measurements of LiI-doped $Li_2S+GeS_2+B_2S_3$ glasses were performed to investigate the ion hopping dynamics and the non-Arrhenius conductivity behavior that has also been observed in some silver fast-ion-conducting (FIC) glasses. The NMR NSLR experiments were performed at 4 and 8 MHz and at 70 kHz in the rotating frame over a temperature range of 183–523 K. Conductivity measurements on these glasses were performed over the same temperature range to determine if the commonly observed non-Arrhenius ionic conductivity in silver FIC glasses was also observed in lithium FIC glasses. Our previously developed distribution of activation energies (DAE) model was used to fit both the NSLR and conductivity results. It was found that a bimodel DAE was required to fit the broad NSLR maximum. One DAE was associated with lithium ions residing in anion sites created by tetrahedral boron units in the thioborate structural regions of the glass, and the other was associated with lithium ions residing in the anion sites created by the nonbridging sulfur units in the thiogermanate regions of the glass. The average activation energy for the lithium ions residing in the thioborate and thiogermanate sites in the ternary glasses agreed very well with the average activation energies for lithium ions in pure binary thioborate and thiogermanate glasses, respectively, with the thiogermanate energies being significantly larger (~45 vs ~30 kJ/mol, respectively) than those for the thioborate sites. This trend is in agreement with the fact that the thiogermanate structures possess nonbridging sulfur units whereas the thioborate structures do not. It was found that some of the non-Arrhenius conductivity behavior could be associated with the bimodal DAE and the conductivity could be fit for the most part with the DAE model. However, the strong deviation from Arrhenius behavior at high temperature could not be accounted for and an extension of the DAE model was therefore included. We consider the effect of a small fraction of mobile ions which are thermally excited above the barriers and are assumed to conduct around many (temperature-dependent) filled sites before reaching a second unoccupied site. This ion-trapping model explains well the high-temperature deviation of the conductivity from Arrhenius behavior.

DOI: 10.1103/PhysRevB.72.144301 PACS number(s): 66.10.Ed, 61.43.Fs, 72.80.Ng, 76.60.Es

I. INTRODUCTION

Fast-ion-conducting (FIC) glasses have received much attention for their potential for use in batteries and fuel cells.[1–5] It has been discovered, however, that many of these highly conducting glasses also show a non-Arrhenius behavior (downward negative curvature) in the conductivity at higher temperatures.[6–13] NMR and ionic conductivity measurements have been used to gain valuable insight into the nature of the ionic motion in these glasses, and it has been well established that the dc conductivity in FIC glass systems is the result of the decoupling of the motions of the weakly bound cations from the host network comprised of, for example, B, Ge, and Si bonded together by oxygen or sulfur.[14–18] Models have been developed to explain the conductivity and NMR data for these conductive materials. To date, the Kohlrausch-Williams-Watts (KWW) function[19–22] and a distribution of activation energies[9,23–26] (DAE) have been two of the more commonly used models to describe the NMR and conductivity data. For Arrhenius FIC glasses, for example, we have made great progress in developing a unified model that can simultaneously fit both the conductivity and the NMR nuclear spin-lattice relaxation (NSLR) data using a single set of DAE parameters.[9,26] However, neither model can fully explain the deviation from Arrhenius behavior of the conductivity at high temperature recently observed in optimized silver FIC glasses.[6]

In this paper, we explore whether the non-Arrhenius conductivity behavior is limited to only optimized silver FIC glasses or whether it is more broadly observed in other ion-conducting glasses such as the lithium thioborogermanate glass reported here. Second, we also seek to explore the role that mixed glass formers might have upon the non-Arrhenius conductivity by comparing the conductivity behaviors of the binary thioborate and thiogermanate glasses to the ternary glasses studied in the present work. It is presumed that the structure of the ternary thioborogermanate glasses will be built up from mixtures of the individual thioborate and thiogermanate structures and this might in turn lead to a requirement to model the transport data using a bimodal DAE, one for the thioborate and one for the thiogermanate structures in the ternary glasses. Such a treatment was implied in our study of the binary thioborate and thiogermanate glasses, where distinct DAE were used for the different glasses. Hence, the structural complexity of the ternary

glasses may therefore lead to a more complex (non-Arrhenius?) temperature dependence of the conductivity.

Our approach is based upon our previous success in using the ^{7}Li NMR NSLR measurements to determine the landscape of barriers and wells experienced by the diffusing ions which is modeled in terms of a DAE.[26] This DAE is then truncated at a typical percolation limit ($\sim$35%–40% for three-dimensional conduction) to calculate the conductivity. In the present case of the presumed bimodal DAE for the ternary glasses, the truncation will be over the complete bimodal DAE and hence yield an asymmetric DAE that may in turn lead to the non-Arrhenius conductivity behavior. It is noted that such combined NMR and conductivity studies have been performed on the ternary silver FIC glasses that were first observed to exhibit the non-Arrhenius behavior.[27] However, the low sensitivity of the ^{109}Ag NMR resonance makes high-precision NSLR measurements very difficult, and for this reason sufficient precision could not be obtained to enable meaningful treatment of the DAE models employed successfully for the lithium glasses.

This study will show for the first time that the non-Arrhenius conductivity behavior is indeed a general phenomenon for both silver and lithium FIC glasses. However, it will also show that while some of the non-Arrhenius behavior in the conductivity can be attributed to a complex (asymmetric) DAE, additional features of the conduction process are necessary to describe the full non-Arrhenius behavior of these FIC glasses. Adding the feature that a small temperature-dependent fraction of the mobile cations are thermally activated into a "free conduction band" in turn leads to the natural result that this fractional population of "free" carriers must travel a temperature-dependent distance before finding an open site (trap). For example, more carriers are thermally activated at higher temperatures, thus creating more open and available sites. This temperature-dependent conduction distance is most prevalent at higher temperatures and is found to account for all of the non-Arrhenius temperature dependence in the conductivity. Conversely, however, we find that the effect of the "free" carriers does not show up conclusively in the ^{7}Li NSLR results. While an abbreviated description of the ion-trapping model (ITM) is provided here, for a more complete description, the reader is referred to Ref. 6.

II. EXPERIMENT

A. Sample preparation

The glass compositions prepared in this study were made by melting stoichiometric amounts of high purity LiI (Aldrich 99% purity), Li_2S (Cerac 99.9% purity), GeS_2, and B_2S_3. Both GeS_2 (Ref. 28) and B_2S_3 (Ref. 29) were prepared by mixing and reacting germanium metal and amorphous boron metal, respectively, with sulfur in sealed silica ampoules that were not and were, respectively, coated with a thin layer of pyrolytic carbon. The coating is required to keep the B_2S_3 from reacting with the silica ampoule at elevated temperatures. All preparations were performed inside a high-purity helium-filled glove box with <5 ppm O_2 and H_2O. Each sample was then mixed and melted in a vitreous carbon crucible at 850 °C for 10 min. Weight loss was then recorded (typically less than 4%), and the sample was then reheated for another 5 min. The resulting liquids were poured into a graphite mold preheated to 200 °C, $\sim T_g - 50$ °C. Samples quenched into brass molds would tend to fracture or stick to the mold depending on the annealing temperature, whereas graphite molds allowed higher quenching and annealing temperatures without the samples sticking. Samples for the NMR experiments were then crushed to a fine powder and sealed into an evacuated quartz tube. Samples for the conductivity experiments were annealed at 200 °C for 30 min and then allowed to cool to room temperature at 5 °C/min. The disks were then sputter coated with gold on both sides to form blocking electrodes for the conductivity experiments. The sputtering was performed at a pressure of 10^{-1} mbar of argon with a current of 18 mA for a total of 4 min on each side.

TABLE I. Density and ion concentration for ternary $z\mathrm{LiI}+(1-z)[x\mathrm{Li_2S}+(1-x)(0.5\mathrm{B_2S_3}+0.5\mathrm{GeS_2})]$ glasses.

Sample	Density (g/ml) +0.06	Calculated total ion concentration (number/m^3) c_0
$x=0.35$	2.19	1.028×10^{28}
$x=0.45$	2.23	1.467×10^{28}
$z=0.0$, $x=0.55$	2.20	1.943×10^{28}
$z=0.1$, $x=0.55$	2.28	1.878×10^{28}
$z=0.2$, $x=0.55$	2.37	1.828×10^{28}
$z=0.3$, $x=0.55$	2.59	1.875×10^{28}

B. Density measurements

Density measurements were made using Archimedes' principle.[30] These measurements were necessary to estimate the ion concentration in the samples needed to model the conductivity data. Results are shown in Table I.

C. dc conductivity measurements

Complex impedance measurements were performed using a Solartron 1260 ac impedance spectrometer. The measurements were made by applying a sinusoidal voltage (50 mV) across the sample. Measurements were made from 180 to 520 K over a frequency range of from 0.1 Hz to 10 MHz. The temperature was controlled to within 1 °C by placing the sample into a specially designed wide-temperature-range cryostat capable of reaching temperatures as low as 100 K to as high as 723 K. Temperature control was accomplished by passing precooled or preheated helium gas through a tube wrapped with band heaters. Temperature scans were made every $\sim$12 °C. Individual frequency scans were not started until the standard deviation of the temperature was within 0.07 °C for the last 30 points measured every 2 sec. The total time for the frequency sweep of the impedance was comparable ($\sim$1 min) to the time observed ($\sim$1 min) for temperature stabilization. Complex plane (Nyquist) plots of the complex impedance so measured were used to determine

the dc impedance from which the dc conductivity was determined.

D. NSLR NMR measurements

All NMR samples were sealed under vacuum in quartz tubes using an oxygen and propane torch to prevent sample contamination with oxygen and water during the measurements. ^{7}Li NSLR T_1 measurements were performed at Larmor frequencies of $\omega_L/2\pi=4$ and 8 MHz over a temperature range of 180–520 K. A phase-coherent pulse NMR spectrometer was used which implemented a programmable pulse sequencer designed by Adduci and Gertstein.[31] This spectrometer used a double-sideband rf switch, and a fast-recovery receiver was used to retrieve the signal.[32] Temperature scans in the NMR experiments were obtained by placing the sample into a custom-built high-temperature probe ($T_{\max}\sim 500$ °C) which used a furnace cavity placed inside a vacuum-jacketed sleeve, with a variable-temperature chamber. All measurements were performed when the temperature control was stable to within 1 °C. The furnace employed r esistive heating, but dry nitrogen gas could also be passed through the probe as a heat exchanger to help facilitate cooling.

The ^{7}Li NSLR measurements were made using either saturation recovery or inversion recovery methods. Both methods were compared at different temperatures and were found to be in good agreement. Saturation recovery consisted of a saturation pulse followed by a 90° read pulse which was typically 2 μs long. The spectral width of the radio frequency pulses was sufficiently wide to excite both the central $(1/2\leftrightarrow -1/2)$ and satellite $(\pm 3/2\leftrightarrow \pm 1/2)$ transitions of the ^{7}Li nuclei so that a single-exponential recovery of the nuclear magnetization was observed in all cases. At all temperatures, the acquisition delays were set to be at a minimum of 10 times T_1.

$T_{1\rho}$ measurements were also performed using a 3.6-μs 90° pulse followed by a spin-locking pulse. This method allows for the measurement of NSLR rates at an effective frequency in the rotating frame $\omega_1=\gamma H_1$, where H_1 is the intensity of the rf field. While the spin-locking pulse is on, the magnetization aligned along the H_1 direction in the rotating frame no longer decays in a time characterized by the spin-spin relaxation, T_2, process. Instead it decays with a time $T_{1\rho}$, corresponding to a spin-lattice relaxation time at an effective frequency $\omega_1=\gamma H_1=70$ kHz.[33] By varying the length of the spin-locking pulse, a value for $T_{1\rho}$ was extracted from the exponential decay of the NMR signal measured at the end of the spin-locking pulse.

III. SUMMARY OF THE THEORETICAL MODELS

A. Distribution of activation energies model of the NMR NSLR and the dc conductivity

It has been found that the correlation times for ionic hopping motion as derived from NMR and conductivity measurements differ by approximately an order of magnitude, with τ_{NMR} being the longer of the two.[20,26,34–36] The NMR correlation time τ_{NMR} is determined by the BPP theory[37] which gives $\tau_{NMR}\sim 1/\omega_L$ at the maximum of the NSLR curve versus $1/T$. The correlation time for conductivity, τ_σ, is determined by $\tau_\sigma\sim 1/\omega(2\sigma_{dc})$ at the frequency above the dc plateau where the conductivity starts to increase. While several theoretical models have been proposed to account for the discrepancy,[34,38] we have shown that by incorporating a simple DAE with a percolation threshold it is possible to account for this discrepancy in a physically understandable manner using a single parameter set.[26] The major assumption of this approach is that the ions present in the glass reside on a set of chemical sites that have differing energy barriers. This assumption is valid in view of known structural disorder of a glass that gives rise to barriers seen by hopping ions that vary in height and depth from site to site.

As described by Kim *et al.*[26] this DAE leads to a distribution of correlation times which then can be used to predict the NLSR and conductivity behaviors as a function of temperature. Equations (1)–(7), below, give the temperature and frequency dependences of the NSLR and the temperature dependence of the dc conductivity and average and individual relaxation times, respectively. While the reader is directed to Ref. 26 for a more complete description of the model, the prefactors for the individual relaxation times τ_{0a}, Eqs. (6) and (7), were taken as a function of the depth of the particular energy well ΔE_a, the mass of the mobile cation, m, and the average distance to the "cusp" of the energy well between adjacent sites, l, estimated from the composition to be ~4 Å:

$$R_1(\omega_L,T)=C\int_0^\infty\left[\frac{\tau_a}{1+\omega_L^2\tau_a^2}+4\frac{\tau_a}{1+4\omega_L^2\tau_a^2}\right]Z_{NMR}d\Delta E_a, \tag{1}$$

$$R_{1\rho}(\omega_1,\omega_L,T)=C/2\int_0^\infty\left[3\frac{\tau_a}{1+4\omega_1^2\tau_a^2}+5\frac{\tau_a}{1+\omega_L^2\tau_a^2}+2\frac{\tau_a}{1+4\omega_L^2\tau_a^2}\right]Z_{NMR}d\Delta E_a, \tag{2}$$

$$\sigma_{dc}(T)=\frac{NPe^2l^2}{6k_BT\tau_{avg}}, \tag{3}$$

$$\tau_{avg}(T)=\frac{1}{P}\int_0^{\Delta Ep}\tau_a(\Delta E_a,T)_{ZNMR}(\Delta E_a)d\Delta E_a, \tag{4}$$

$$\tau_a=\tau_{0a}\exp\left(\frac{\Delta E_a}{k_BT}\right), \tag{5}$$

$$\tau_{0a}=1/6r_{0a}, \tag{6}$$

$$r_{0a}=(\Delta E_a/2m)^{0.5}/l. \tag{7}$$

B. Ion trapping model of the non-Arrhenius dc conductivity

It will be shown below that while the DAE model can account simultaneously for the NMR NSLR data and for

some of the non-Arrhenius behavior in the dc conductivity, it cannot account for all of the non-Arrhenius behavior. For this reason, a simple, but important extension of the DAE model was added that enables the strong non-Arrhenius temperature dependence of the dc conductivity to be modeled. The ITM, which accurately fits the conductivity data for glasses (such as those presented here) and crystals showing non-Arrhenius behavior in the conductivity, suggests that once an ion is thermally activated, it must travel a temperature dependent distance (up to 10 Å) before it is recaptured into another cation site (trap). This model is distinct from other models where a cation performs a single hop to the next-neighboring location, which is on the order of only a few Å's away. A brief explanation of this model is given here. For a more complete discussion the reader is referred to the paper by Martin *et al.*[6]

Given a system with a concentration c_0 of cations that can be thermally activated to hop, the fraction of ions that are thermally promoted to conduction is given by Boltzmann statistics in Eq. (8), where ΔE_a is the activation energy, k_B is Boltzmann's constant, T is temperature, and $c(T)$ is the temperature-dependent concentration of ions, which will be assumed to diffuse freely in the lattice for a few nanometers before being trapped again into a well:

$$c(T) = c_0 e^{-\Delta E_a / k_B T}. \tag{8}$$

Using the average thermal drift velocity and the additional drift velocity created by the applied electrical field gradient, the conductivity, which is given by the current density (the product of the net ion drift velocity, the number of actual charge carriers, and the area through which the conduction occurs) divided by the electric field gradient becomes

$$\sigma = \frac{c(T) q^2 \lambda(T)}{\sqrt{\frac{2mk_B T}{3}}}. \tag{9}$$

The mean free path $\lambda(T)$ is taken to be the reciprocal of the additive inverses of two mean free paths, λ_0 and $\lambda_1(T)$. In this model, it is hypothesized that as a cation is migrating through the glass network, it experiences both repulsive and attractive forces due to the other cations and anions, respectively. As the mobile cation increasingly approaches an anion, the attractive forces become greater and ultimately pull the cation into the trap (neighboring anion site). Because the number of cations is temperature dependent, $\lambda_1(T)$, the temperature-dependent mean free path is calculated in Eq. (10) from the concentration of Coulombic traps created by the thermal excitation of cations from their equilibrium sites and the trapping cross section of the interaction, πd^2, where d is a measure of the capture cross section of the cation site that depends upon its charge density and the thermal velocity of the mobile cation:

$$\lambda_1(T) = \frac{1}{\sqrt{2}\pi d^2 c_0 \exp\left(\frac{-\Delta E_a}{k_B T}\right)}. \tag{10}$$

In Eq. (11), d is calculated by equating the electrostatic force between an anion and cation to the centripetal force experienced by a moving cation at a distance d away from the center of an anion site:

$$d = \frac{e^2}{8\pi\varepsilon_0\varepsilon_\infty kT}. \tag{11}$$

Since the concentration of traps is temperature dependent, this would lead to an infinite mean free path at $T=0$ K (zero "free" carriers). To avoid this unacceptable result, λ_0 is introduced to create a low-temperature mean-free-path maximum. Hence, $\lambda(T)$ becomes

$$\lambda(T) = \left[\frac{1}{\lambda_0} + \frac{1}{\lambda_1(T)}\right]^{-1}. \tag{12}$$

At low temperatures, λ_0 is much smaller than λ_1 and therefore dominates as the overall mean free path. As temperature increases, the number of cation traps increases at the same rate that new ions are thermally activated. It can be shown from Eq. (10) that at higher temperatures, λ_1 eventually becomes smaller than λ_0 and dominates the behavior of the mean free path $\lambda(T)$. The cation traps can be thought of as the vacant sites from which the ions were activated. When an ion comes within the vicinity of these charged vacant sites, it is attracted by the Coulomb force between the mobile cation and immobile anion (trap).

It should be noted that the concept of the ITM is similar to variable-range hopping introduced by Mott for electronic conduction in glasses containing transition metal ions.[39,40] A similar model has also been previously suggested by Rice and Roth.[41]

IV. RESULTS

A. ^{7}Li NSLR

At room temperature and above, only one narrow ^{7}Li NMR central line was observed in the absorption spectra at both 4 and 8 MHz. At these temperatures, the normally observed broader line associated with the satellite transitions affected by the distribution of local electric field gradients is narrowed due to the fast motion of the Li^+ ions in these glasses. Therefore, as reported by Kim *et al.*,[26] all of the relaxation measurements yielded a single-exponential recovery.

Figure 1 shows the ^{7}Li NSLR rates $R_1(\omega_L, T) = 1/T_1(\omega_L, T)$ and $R_{1\rho}(\omega_1, T) = 1/T_{1\rho}(\omega_1, T)$ on a semilogarithmic plot for the $z=0.0$ and $x=0.55$ glass. On the low-temperature side of the $R_1(\omega, T)$ maximum, the asymmetry in the curve is due to the structural disorder in these materials and this behavior has been explained by the DAE model proposed by Kim *et al.*[26] Also shown in the figure are the $1/T_{1\rho}$ measurements for the same sample at an effective frequency in the rotating frame $\omega_1 = \gamma H_1 = 70$ kHz where H_1 is the intensity of the radio frequency (rf) field.

Examining the relaxation rate curves, it is found that the $z=0.0$ and $x=0.55$ glass exhibited a very broad maximum at approximately 420 K. The maximum relaxation rates were

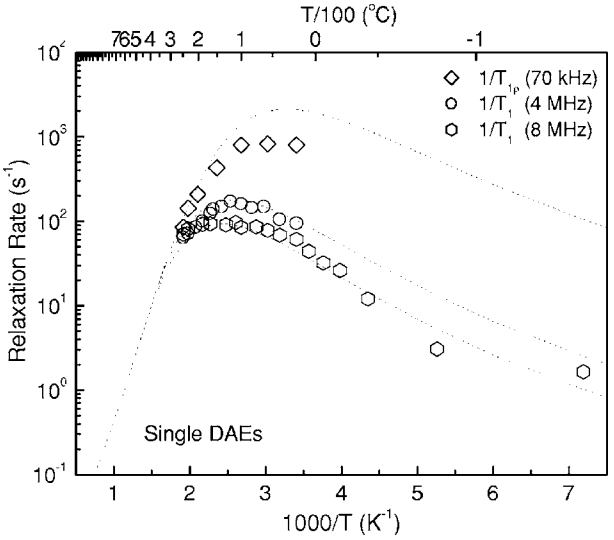

FIG. 1. Fit of single DAE to NSLR data for $0.55Li_2S+0.45(0.5B_2S_3+0.5GeS_2)$ glass at the three frequencies measured according to Eqs. (1)–(7) with $\Delta E_m=41.6$ kJ/mol and $\Delta E_b=15.0$ kJ/mol.

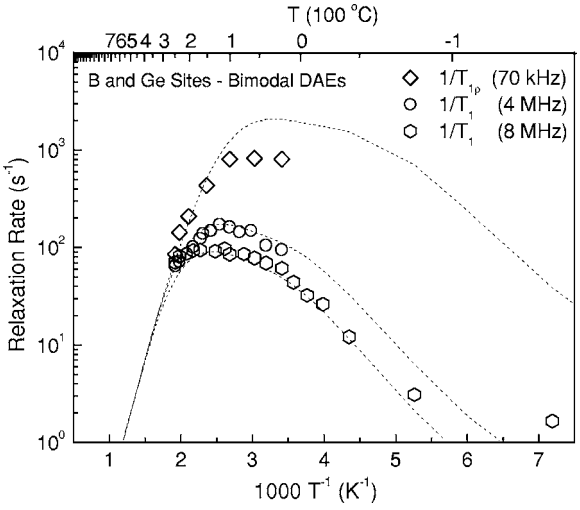

FIG. 2. NSLR measurements of Fig. 1 with fits using two Gaussian DAE, one for Li^+ ions in boron sites and another for Li^+ ions in Ge sites for the $0.55Li_2S+0.45(0.5B_2S_3+0.5GeS_2)$ glass. Values of parameters used to obtain best-fit are given in Table II.

approximately 100 and 150 ms^{-1} for the 4 and 8 MHz curves, respectively. At higher temperatures the relaxation curves appear to coalesce into a common straight line upon which the slope represents the average activation energy of the ionic species in the sample. It is noted that in order to investigate the consequences of the ITM on NSLR one should extend the measurements to much higher temperatures, which is prevented in our samples by the crystallization processes. The asymmetry in the logarithmic plot of the NSLR vs $1/T$ and the deviation from the ω^{-2} dependence at low temperatures predicted by the BBP theory[37] in the presence of a single correlation time is accounted for in the DAE model as shown in the fits discussed below based on Eqs. (1)–(7). The NSLR data were fitted (dashed lines) using 4 Å for the jump distance l in Eq. (3), which is slightly smaller than the calculated ion separation distance based on composition. Here and for the moment a fixed jump distance is consistent with our and all other previous models. The parameters ΔE_m, ΔE_b, and C were then adjusted to yield good fits of the NSLR data at all frequencies measured. The DAE model for the NSLR data gives a good agreement using the parameters that were derived from the NMR measurements.

For the data shown in Fig. 1, fitting the NSLR data with a single DAE required an average activation energy (ΔE_m) of 41.6 kJ/mol and a distribution width (ΔE_b) of 15.0 kJ/mol. Such a broad distribution was not surprising; it was expected that a large width would be needed to account for the range of different cation sites (structures) produced in a glass with two different glass formers (B_2S_3 and GeS_2). While the fit to the NSLR data with a single DAE was reasonably good, careful inspection of Fig. 1 shows that the full breath of the data [full width at half maximum (FWHM)] could not be well fitted without having a large overshoot on the low-temperature side of the data, seen most clearly in the 8-MHz data. For this reason, a fit to the NSLR data with two DAE, one for each of the sets of cation sites produced by the two different glass formers $BS_{4/2}^{-1}$ and $GeS_{3/2}S^{-1}$, was used to more accurately fit both the high- and low-temperature sides of the NSLR data as shown in Fig. 2. With the two DAE shown in Fig. 3, the fit is improved in that the FWHM of the curve is better accounted for and there is less of a low-temperature overshoot, as seen Fig. 2. To quantify the deviation between the two fits single and bimodal DAE, the root-mean-square deviation of the NSLR data was calculated and the fit using a bimodal DAE was on average 5% better than that of the fit using a single DAE.

Such bimodal DAE are known and have been previously used when the glass chemistry is such that it naturally produces multiple glass subnetworks. For example, Kim *et al.*[42,43] found that it was necessary to use two DAE to fit the relaxation curves in binary lithium thioborate glasses where the two separate distributions describe two different sets of cation sites produced by boron atoms in trigonal ($BS_{2/2}S^{-1}$) and tetrahedral coordination ($BS_{4/2}$), respectively. In this

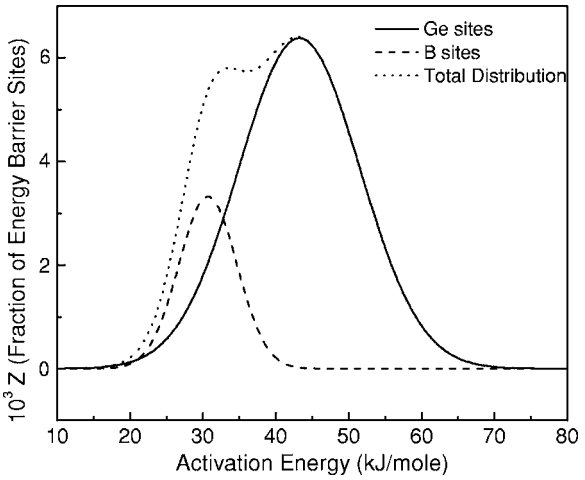

FIG. 3. Total DAE using two separate Gaussian DAE used in fitting NSLR data for $0.55Li_2S+0.45(0.5B_2S_3+0.5GeS_2)$ glass.

TABLE II. Average activation barriers ΔE_m (kJ/mol) and corresponding standard deviations ΔE_b (also in kJ/mol and in parentheses), determined from NSLR measurements using a bimodal DAEs fit in $z\mathrm{LiI}+(1-z)[x\mathrm{Li_2S}+(1-x)(0.5\mathrm{B_2S_3}+0.5\mathrm{GeS_2})]$ glasses.

Composition	Germanium site binary[a]	Germanium site ternary	Tetrahedral boron site binary[b]	Tetrahedral boron site ternary
$x=0.35$	50.72 (9.15)	49.88+1.66 (9.15+0.83)		34.92+0.83 (5.40+0.42)
$x=0.45$	46.97 (9.15)	45.73+1.66 (9.15+0.83)		33.26+0.83 (4.49+0.42)
$x=0.55$	41.57 (8.31)	42.40+1.66 (8.31+0.83)		30.76+0.83 (3.99+0.42)
$x=0.65$			28.52 (2.99)	
$x=0.7$			27.44 (2.16)	
		Germanium site quarternary		Boron tetrahedral site quarternary
$z=0.1$, $x=0.55$		42.40+1.66 (8.31+0.83)		30.76+0.83 (3.33+0.42)
$z=0.2$, $x=0.55$		40.74+1.66 (8.31+0.83)		30.76+0.83 (3.66+0.42)
$z=0.3$, $x=0.55$		39.91+1.66 (8.31+0.83)		30.76+0.83 (3.33+0.42)

[a]Reference 26.

[b]References 25 and 42.

present study the two DAE needed to fit the data represent lithium ions that are associated with germanium sites ($\mathrm{GeS_{3/2}S^{-1}}$) and tetrahedral boron sites ($\mathrm{BS_{4/2}^{-1}}$), respectively. While it is reasonable to suggest that there might be some boron sites in trigonal coordination that also have lithium ions associated with them, such as the $\mathrm{BS_{2/2}S^{-1}}$ sites found in binary all-thioborate glasses, the ^{11}B NMR spectra of these ternary (and quaternary) glasses, however, show that ~80% of the boron atoms are in tetrahedral ($\mathrm{BS_{4/2}}$) coordination.[44] While it could be thought that such a large number of tetrahedral borons would accordingly be associated with an equally large number of charge-compensating Li ions, this is not the case. In these thioborates, the sulfur goes into threefold coordination to produce the large number of tetrahedral borons and in doing so is able to create neutral tetrahedral borons.[44] Of the remaining 20% of boron which is in trigonal coordination, if it is assumed that there is an equal number of both trigonal boron atoms with nonbridging sulfurs ($\mathrm{BS_{2/2}S^{-1}}$) and trigonal boron atoms with all bridging sulfur atoms ($\mathrm{BS_{3/2}}$), then only about 5% of the lithium would be associated with nonbridging sulfur atoms on the trigonal boron atoms. Since two distributions are already being used, this extra 5% of different cation sites would not make a significant impact in the shape of the relaxation curves; thus it does not unambiguously improve the fit used. Therefore, a third DAE for lithium ions associated with trigonal boron atoms with a nonbridging sulfur was not included.

Table II gives the parameters, ΔE_m, ΔE_b, and C, in Eqs. (1) and (2), used to give best fits to the NSLR data shown in Figs. 2, 4, and 5 for all of the undoped and the $z=0.2$ LiI doped glasses, respectively. For brevity and clarity, the plot and fit for the $z=0.1$ and 0.3 glasses are not shown. As shown in Figs. 6 and 7, the activation energy ΔE_m and its standard deviation ΔE_b decrease for both the germanium and boron sites with increasing $\mathrm{Li_2S}$ in the undoped glasses and with increasing LiI in the doped glasses. For the germanium sites in the ternary glasses, values very similar to those of the germanium sites in the binary $\mathrm{Li_2S+GeS_2}$ glasses were observed, as shown in Fig. 6. In the case of the boron sites,

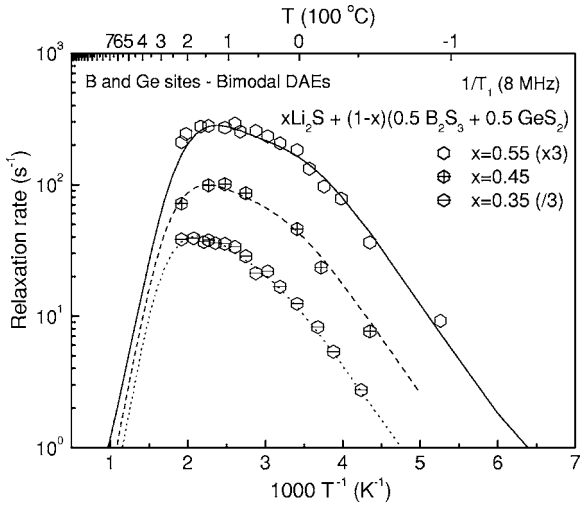

FIG. 4. DAE fits to NSLR data for $x=0.35$, 0.45, and 0.55 ternary glasses using two DAE for lithium ions in boron and germanium sites using the activation energy and coupling constant values given in Tables II and III, respectively. Curves for the 0.35 and 0.55 glasses were offset for clarity as shown in the legend to the figure.

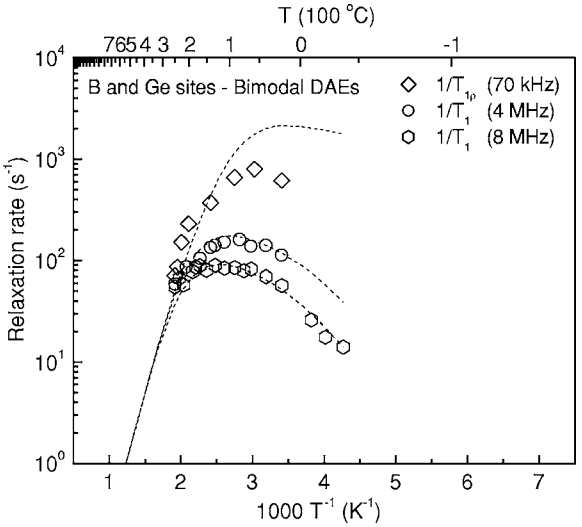

FIG. 5. NSLR data and fits for $0.2\text{LiI}+0.8[0.55\text{Li}_2\text{S}+0.45(0.5\text{B}_2\text{S}_3+0.5\text{GeS}_2)]$ glass using two DAE and coupling constant values taken from Tables II and III, respectively. For brevity, data and plot for the $z=0.3$ LiI glass are not shown, but fitting parameters for the DAE and C are given in Tables II and III, respectively.

direct comparisons cannot be made at similar Li_2S compositions since only binary glasses at the $x=0.65$ and 0.70 compositions were glass forming. However, as Fig. 6 shows, a systematic decreasing trend can be seen when plotting ΔE_m versus composition for $x=0.35-0.7$. ΔE_m decreases from ~50 to ~42 kJ/mol for the thiogermanate sites and from 35 to 31 kJ/mol for the thioborate sites. A slight decrease in ΔE_m was seen with added LiI for the germanium sites, ~42 to ~40 kJ/mol, while ΔE_m for the boron sites remained unchanged at ~31 kJ/mol. Agreement between the activation energy data for the germanium glasses and the

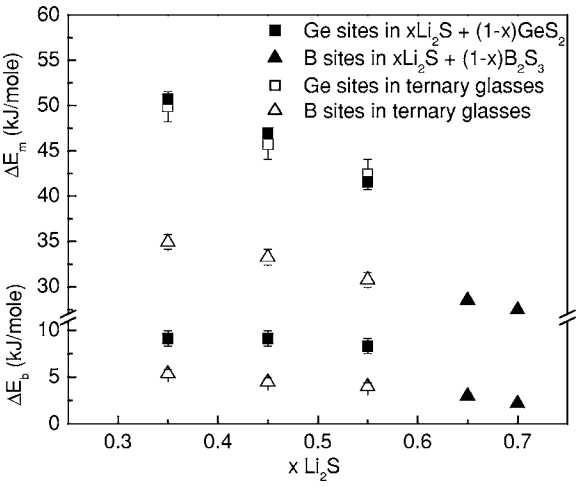

FIG. 6. Average activation energies (ΔE_m) and standard deviations (ΔE_b) determined for DAE fits to the NSLR measurements data as a function of Li_2S content. Values for binary $x\text{Li}_2\text{S}+(1-x)\text{GeS}_2$ glasses (filled squares, $x=0.35$, 0.45, and 0.55) are taken from Ref. 26. Values for the binary $x\text{Li}_2\text{S}+(1-x)\text{B}_2\text{S}_3$ glasses (filled triangles, $x=0.65$ and 0.70) are taken from Ref. 25.

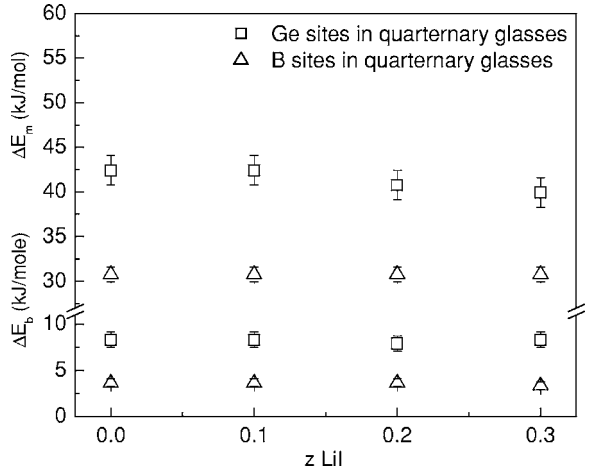

FIG. 7. Average activation energies (ΔE_m) and standard deviations (ΔE_b) determined for DAE fits to the NSLR measurements data as a function of LiI content for $z\text{LiI}+(1-z)[0.55\text{Li}_2\text{S}+0.45(0.5\text{B}_2\text{S}_3+0.5\text{GeS}_2)]$.

extrapolated data for the borate glasses is very good. Binary lithium thioborate glasses cannot be prepared for x less than 0.5 due to phase separation. The addition of GeS_2 and other glass formers such as GeO_2 and As_2S_3 can be used to close this miscibility gap, but unfortunately also limit the range of conventional glass formation and for this reason were not explored in the present work.

Significantly, it is observed that the germanium sites have the larger of the two activation energies, ~50 to ~42 kJ/mol compared to ~35 to ~31 kJ/mol. Such behavior is perhaps reasonable in view of the fact that the germanate structures are expected from Raman and IR spectroscopy[44] to possess terminal and fully charged nonbridging sulfurs whereas the thioborate structures are expected to be comprised of tetrahedral boron units where the negative charge is distributed evenly over four bridging sulfurs. It is therefore expected that the thioborate units would have a smaller charge density than the thiogermanate units and as such produce a smaller activation energy barrier.

Similar to the germanium sites in the binary glasses, the width ΔE_b of the DAE for the germanium sites in the ternary glasses does not change significantly with added Li_2S from $x=0.35$ to 0.55, as shown in Fig. 6. However, there is a decrease from ~5 to ~4 kJ/mol in the width of the DAE for the tetrahedral boron sites over the range of x from 0.35 to 0.55 in the ternary glasses. For the LiI-doped glasses, no significant change in the distribution width was observed.

Some assumptions had to be made when determining the values for the coupling constants C in Eqs. (1) and (2). The first assumption was that the environments that the lithium ions experience around the germanium and boron sites in the ternary glasses will probably not differ significantly from the corresponding sites in the binary glasses. Hence, the coupling constants C in the ternary glasses were taken to be approximately the same as the values for the corresponding binary glasses. The values for C are shown in Fig. 8 as a function of x Li_2S. The total relaxation rate R_{total} was then fitted by taking a weighted average of the relaxation times for both the germanium sites and boron sites in the ternary

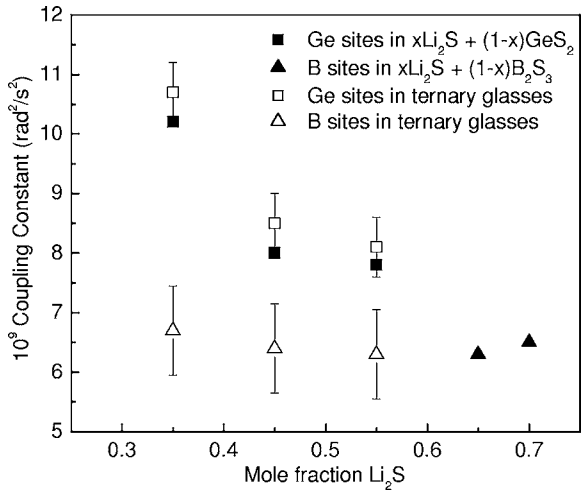

FIG. 8. Coupling constants determined by NSLR measurements and DAE fits of the NSLR measurements for the ternary glasses compared to the values obtained for binary lithium thio-germanate and lithium thio-borate binary glasses. Data for the binary thio-germanate and thio-borate glasses taken from Refs. 26 and 25, respectively.

glasses. The two sites are weighted according to the fraction of lithium ions associated with them. The sum of the fraction parameters f_1 and f_2 in Eq. (13) would equal 1 to account for all of the lithium ions in the glasses. This effectively creates a weighted average of the two DAE to give the overall measured relaxation curve. The total relaxation is given by Eq. (13):

$$R_{total}(\omega_L,T) = f_1^* R_1(\omega_L,T) + f_2^* R_2(\omega_L,T) \qquad (13)$$

Values for the coupling constants, which are embedded in the R_1 and R_2 terms in Eq. (13), used in the fits are shown in Table III and in Fig. 8. The coupling constant values were optimized to yield a best fit to the data and reveal that the lithium atoms are distributed such that 70%–80% of the lithium ions undergo relaxation around germanium sites, while the remaining 20%–30% relax around boron sites. Equal sharing based on composition alone would suggest ~33% of the lithium to be associated with germanium sites and ~67% to be associated with boron sites since the ratio of germanium to boron is 1:2. However, the preference of lithium ions to distribute heavily toward germanium sites is in agreement with the qualitative results shown by IR and Raman spectra taken of these glasses.[44] This distribution, which favors the germanium sites, is also in agreement with that expected from energetics. The sites with the higher binding energy towards lithium would naturally bind more readily to the available lithium ions than the sites with the lower binding energies. Significantly however, it is expected that the more mobile lithium ions will come from the lower-binding-energy sites, the thioborate sites.

B. dc conductivity results

The dc conductivity values were determined by using a Nyquist plot shown in Fig. 9 and extrapolating the imaginary part of the complex impedance to the x-axis intercept along the real impedance axis. Figure 10 shows an Arrhenius plot of the dc conductivity for the LiI-doped $x=0.55$ series of glasses and one $x=0.45$ glass for comparison. The highest conductivity measured at room temperature is between 10^{-3} and 10^{-4} $(\Omega\,\mathrm{cm})^{-1}$. With increasing Li_2S content, the activation energy decreases. This can be seen by the changes in slope of the data curves on the Arrhenius plot. As predicted by the NMR data where a lower activation energy was observed for the LiI-doped glasses, the addition of LiI causes a slight decrease in the conductivity activation energy. Likewise and similar to the silver FIC glasses,[13,45,46] the addition of LiI increases the conductivity. As is also similar to the silver FIC glasses, the glasses in this study show an increasing deviation (more curvature) from Arrhenius behavior with increasing LiI content.[45,46]

In an effort to rule out electrode, oxidation, and/or other spurious effects as giving rise to the non-Arrhenius behavior,

TABLE III. Coupling constants C $[10^{-9}\ (\mathrm{rad/sec})^2]$, determined by NSLR measurements and DAEs fit for $z\mathrm{LiI}+(1-z)[x\mathrm{Li_2S}+(1-x)(0.5\mathrm{B_2S_3}+0.5\mathrm{GeS_2})]$ glasses.

Composition	Germanium site binary[a]	Germanium site ternary	Tetrahedral boron site binary[b]	Tetrahedral boron site ternary
$x=0.35$	10.2	10.7+0.5		6.7+0.5
$x=0.45$	8.0	8.5+0.5		6.4+0.5
$x=0.55$	7.8	8.1+0.5		6.3+0.5
$x=0.65$			6.3	
$x=0.7$			6.5	
	Germanium site quarternary		Boron tetrahedral site quarternary	
$z=0.1$, $x=0.55$	8.1+0.5		5.5+0.75	
$z=0.2$, $x=0.55$	8.1+0.5		5.5+0.75	
$z=0.3$, $x=0.55$	8.1+0.5		5.5+0.75	

[a]Reference 26.
[b]References 25 and 42.

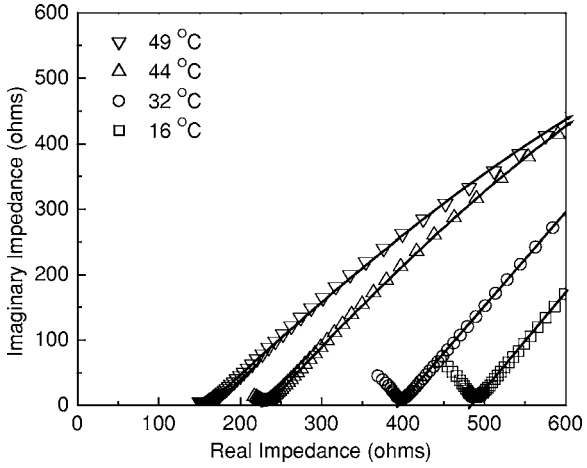

FIG. 9. Nyquist plot of the complex impedance at four selected and intermediate temperatures for the $0.2LiI+0.8[0.55Li_2S+0.45(0.5B_2S_3+0.5GeS_2)]$ glass.

two consecutive temperature scans were performed on the same $z=0.2$, $x=0.55$ sample. The sample was first heated to 200 °C, held for 6 h at 200 °C, and then cooled back to room temperature. This temperature cycle was repeated on the same sample. The conductivities between the two separate heating runs were in exact agreement and exhibited exactly the same extent of non-Arrhenius conductivity temperature dependence.

The dc conductivity was fitted with the DAE model by using the DAE determined by the NSLR NMR measurements described above. The average correlation time τ_{avg} was determined by taking the weighted average of all correlation times corresponding to activation energy barriers from 0 up to a percolation threshold ΔE_p given in Table IV. The value for ΔE_p is determined by best fitting Eqs. (3) and (4) to the dc conductivity data. Again, 4 Å was used for the average jump distance l for reasons discussed above. The ion concentration c_0 was calculated from composition and density measurements shown in Table I. In this treatment, ΔE_p represents the fraction of activation energy barriers at lower values comprising approximately 1/3 of the total distribution of cation sites.

TABLE IV. Percolation fraction values used in fitting the dc conductivity data with the DAE model.

Sample	Percolation fraction	ΔE_p (kJ/mol)	ΔE_m (kJ/mol)
$z=0.0$, $x=0.45$	0.404	39.91	32.90
$z=0.0$, $x=0.55$	0.404	37.08	31.28
$z=0.1$, $x=0.55$	0.312	34.42	29.96
$z=0.2$, $x=0.55$	0.324	33.75	29.31
$z=0.3$, $x=0.55$	0.352	33.75	29.31

The solid lines in Fig. 10 are fits to the conductivity data using the DAE model with a percolation threshold. It can be seen from Fig. 10 that while a reasonable fit to most of the data is found and supports our previous finding that the Arrhenius conductivity can be treated in this way, the DAE model fails to fit the non-Arrhenius behavior of the conductivity at the higher temperatures. However, the DAE model does accurately predict the Arrhenius portion of the dc conductivity plots as we have observed in the past for lower conductivity binary Li_2S+GeS_2 glasses.

For these reasons, we have extended the DAE model to the ITM, which is able to fit both the Arrhenius and non-Arrhenius regions of the dc conductivity very well as shown in Fig. 11. The dc conductivity was fitted using Eq. (9) where ΔE_a was substituted by the integral over the NMR determined DAE, Z_{NMR}. The ion concentration c_0 was calculated from the known composition and density of the glasses

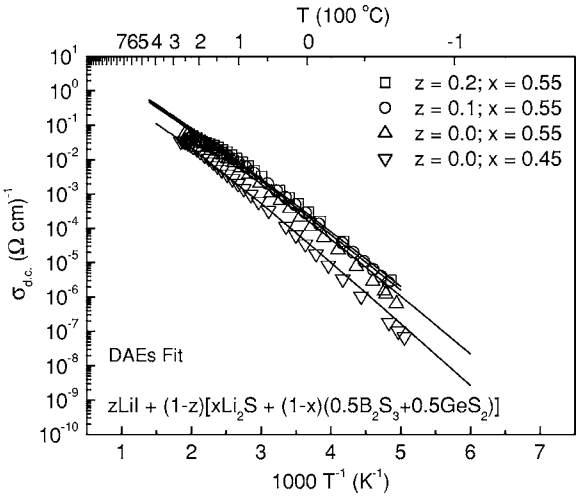

FIG. 10. dc ionic conductivities of the ternary zLiI $+(1-z)[x\mathrm{Li}_2\mathrm{S}+(1-x)(0.5\mathrm{B}_2\mathrm{S}_3+0.5\mathrm{GeS}_2)]$ glasses and fits (solid lines) determined by the DAE to Eq. (2). Note that while the DAE is able to account for some of the non-Arrhenius downward curvature in the conductivity data, it does not account for it completely.

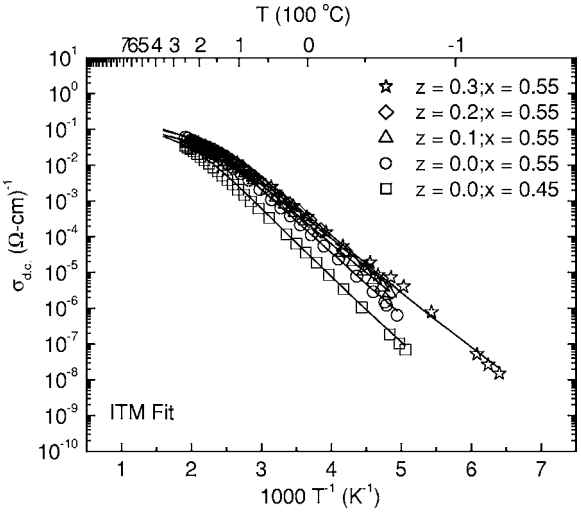

FIG. 11. dc ionic conductivities of the ternary zLiI $+(1-z)[x\mathrm{Li}_2\mathrm{S}+(1-x)(0.5\mathrm{B}_2\mathrm{S}_3+0.5\mathrm{GeS}_2)]$ glasses and fits (solid lines) determined from the ITM model. Values for the parameters used in the ITM model are given in Table V. Note that unlike the simple DAE model, the ITM model is able to completely model all of the non-Arrhenius downward curvature in the conductivity.

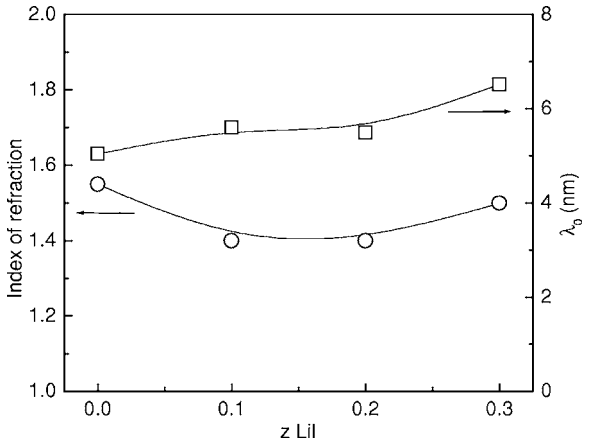

FIG. 12. Composition dependence of the index of refraction values used for fitting the ITM to the dc conductivity for $z\mathrm{LiI}+(1-z)[0.55\mathrm{Li_2S}+(0.45)(0.5\mathrm{B_2S_3}+0.5\mathrm{GeS_2})]$ glasses. The Claussius-Mossoti equation was used to relate the index of refraction to the limiting high frequency dielectric constant of the glass.

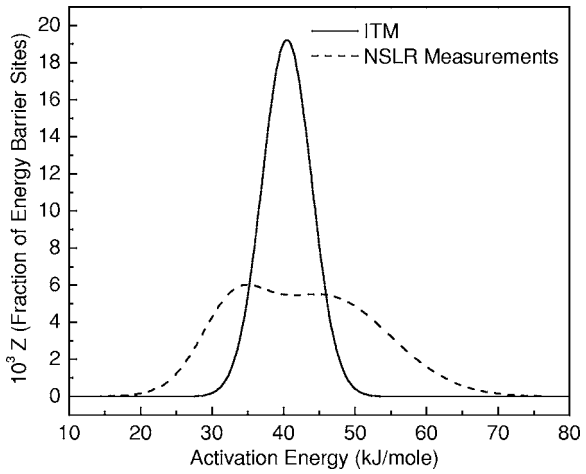

FIG. 13. Comparison between the NMR determined DAE and the DAE needed for fitting with the ITM in $0.2\mathrm{LiI}+0.8[0.55\mathrm{Li_2S}+0.45(0.5\mathrm{B_2S_3}+0.5\mathrm{GeS_2})]$ glass. In the ITM model, we do not *a priori* assume a bi-model distribution as is required in the NSLR fitted data. Significantly, while the average values of each distribution agree well, the width of the DAE for the NSLR data is much wider than that for the conductivity data.

shown in Table I. Since the conductivity in these glasses is high and the ac impedance measurements are limited to 1 MHz, it is not possible to accurately determine values for ε_∞ even at liquid-nitrogen temperatures. We have chosen to use the Lorentz-Mossotti relation $\varepsilon_\infty \sim n_o^2$, where n_o is the index of refraction, to estimate the optical frequency value of ε_∞. In the present case, the index of refraction parameter was allowed to vary for purposes of fitting the data, and in the future refractive index measurements will be made to confirm the values obtained. The values for n_o, the index of refraction, remained at a value of approximately 1.5 regardless of the concentration of LiI, a value not too dissimilar from that expected for these glasses (see Fig. 12). λ_0 values were calculated from the inverse cube root of Eq. (8), where the temperature is set to T_g—viz., taking the fixed trap sites to be frozen in when the glass structure freezes in at T_g. λ_0 increases from 5.5 to 6.6 nm with the addition of LiI as shown in Fig. 12. Figure 13 shows the average activation energy used and its comparison to the weighted average calculated from the NMR determined parameters. The DAE width ΔE_b used in the ITM is quite narrow, $\sim$4 kJ/mol, compared to experimentally determined values by NMR, $\Delta E_b \sim 9$ kJ/mol for the thiogermanate sites, for example. This difference is shown in Fig. 13, where the DAE from NSLR and that used in the ITM to fit the dc conductivity are compared.

V. DISCUSSION

The overarching goal of the present study was to investigate the observation or otherwise of the non-Arrhenius dc conductivity in nonsilver ion-conducting glasses. The combined use of NMR NSLR and dc conductivity measurements in this study was directed at determining whether there might be an underlying strong asymmetry in the DAE that the mobile lithium ions experience in conduction events that would lead to the observed non-Arrhenius conductivity. While a marked asymmetry in the DAE was observed and was the consequence of the mixed glass formers used in this ternary glass forming system under study and while this asymmetry did in turn lead to some measure of non-Arrhenius behavior in the dc conductivity, the full and strong non-Arrhenius behavior was not reproduced. This forced the natural extension of the DAE model to include the possibility that only a small fraction of the mobile ions are thermally excited at any one temperature. Doing so enabled the full non-Arrhenius conductivity behavior to be reproduced.

A. DAE approach to fitting the NSLR NMR and dc conductivity data

The T_1 measurements at all temperatures yielded a single-exponential relaxation curve, and this suggests that all of the lithium atoms were able to reach a common spin temperature during the relaxation process. From these measurements, the fitted parameters from the bimodal DAE model showed that the average activation energy (ΔE_m), distribution width (ΔE_b), and coupling constants (C) for the ternary glasses are consistent with the values for the binary thioborate and binary thiogermanate glasses. The resulting sum of the two DAE yields an overall asymmetric DAE for the ternary and quaternary glasses.

The NSLR data could be well fit using a bimodal DAE for all compositions and all frequencies and even for the LiI-doped glasses where the strongest deviation from Arrhenius conductivity was observed. This suggests that at the level of precision available in the NSLR measurements, the presence of the "free" diffusing ions postulated in the ITM which cause the non-Arrhenius behavior in the conductivity at the highest temperatures does not modify in a measurable way the NSLR temperature behavior as predicted by the DAE model. However, it should be noted that NMR measurements at higher temperatures may be necessary to firmly establish

TABLE V. Parameters used for the ITM of the dc conductivity in $z\mathrm{LiI}+(1-z)[x\mathrm{Li_2S}+(1-x)(0.5\mathrm{B_2S_3}+0.5\mathrm{GeS_2})]$ glasses.

Sample	n_0	λ_0 (nm)	ΔE_m (kJ/mol)	ΔE_b (kJ/mol)
$z=0.0$, $x=0.45$	1.4	6.106	44.06	3.87
$z=0.0$, $x=0.55$	1.55	5.039	40.49	3.45
$z=0.1$, $x=0.55$	1.4	5.604	40.06	3.95
$z=0.2$, $x=0.55$	1.4	5.496	39.49	3.95
$z=0.3$, $x=0.55$	1.5	6.522	38.83	3.74

this point. These measurements are very difficult since the glass transition temperature T_g limits the upper temperature to which measurements can be made and the present measurements were made to as high a temperature as possible for this reason. Another option would be to perform measurements over a wider frequency range. However, moving to higher frequencies causes less of the frequency-independent plateau region to be observed because the peak maximum temperature will shift to higher temperatures at higher frequencies. Regarding the lower frequencies, the value of 4 MHz used here is as low as we could practically go in view of the rapidly decreasing sensitivity of the NMR spectrometer.

One way to obtain measurements of spin-lattice relaxation at very low effective frequencies is to measure $T_{1\rho}$ as was done here at 70 kHz. These measurements, as the data suggest in Figs. 1, 2, 4, and 5, do allow a wider range of temperatures to be probed where the NSLR is expected to be frequency independent and as such should be helpful in exploring the ion dynamics in the region of deviation of the conductivity from Arrhenius behavior. However, since the theory for $T_{1\rho}$ is not as straightforward as it is for T_1, it would be difficult to assign deviations from the DAE model at high temperature to the presence of "free" diffusing ions as done in the ITM for the conductivity. The field-cycling NMR technique allows measurements of NSLR over a wide and nearly continuous range of frequencies, and this technique will be applied to these glasses in the near future and will be reported on separately.

B. Ion trapping model of the non-Arrhenius conductivity

Table V shows the parameters used to fit the data with the ITM. The general trend in the activation energies is as expected and that is to decrease with added Li_2S and LiI. The index of refraction n has a fairly constant value of 1.5, which is expected for these glasses. It is very important, however, that this parameter be confirmed through independent refractive index measurements because it has a significant effect on the value for the effective trapping diameter d. λ_0 gradually increases with added LiI because the average activation energy decreases with added LiI, and this gives rise to a greater number of ions thermally activated at the same temperature when compared to samples with higher average activation energies.

The significant finding here is that the NSLR determined DAE cannot be used in the ITM to produce a good fit to the dc conductivity. This was quite unexpected. It was anticipated that the NMR-determined DAE would be the full and correct one as we have shown for glasses with Arrhenius dc conductivities. However, when the NSLR DAE is used, it produces a significantly higher conductivity than experimentally observed due to its broader energy range, enabling much lower activation energies to be used in calculating the conductivity. A much narrower activation energy distribution is required as shown in Fig. 13 and compared to the NSLR DAE for the $z=0.2$ LiI glass. The result that the average values for the two distributions are almost identical is not surprising since they both are shown to fit the overall trends in the dc conductivity, and hence they both must fit the average slope of the dc conductivity and hence the agreement between the two average activation energy values. However, it must be noted that the DAE approach to calculating the dc conductivity includes a percolation fraction treatment that truncates the distribution to the lower (below the percolation threshold, typically $\sim 30\%-40\%$ as seen in Table III) activation energy values. Hence it might have been expected to observe the ITM DAE centered not at the average of the full NSLR DAE, but rather centered at the average of the percolation threshold truncated distribution.

The ITM makes the important suggestion that the average distance that a mobile ion travels is $\lambda_{trap}(T)$ and that these distances are much larger, nm, than typically thought, just a few Å, for example. It is significant to note that these distances also increase with decreasing temperature. The model suggests that mobile cations migrate through the glass until they arrive at an open site or trap. Since open sites become more numerous the more thermally activated the cations are, the sites must therefore become less numerous at lower temperatures. Hence, on average, the ITM suggests that the cations must travel longer distances at lower temperatures. This is contrary to the perhaps expected behavior where longer diffusional distances would be expected at higher temperatures. At this point, however, we cannot conclusively prove which is the correct behavior. Our result here is that the simply based ITM using a few adjustable parameters can accurately reproduce the non-Arrhenius conductivity behavior of these glasses. We are in the process of exploring methods to experimentally determine the temperature dependence of the average conduction distance and will report on these experiments as they are completed.

It must be noted that this value is an "average" and does not describe specifically the dynamics of the ions individually. It could be possible, for example, for a large number of ions to travel very short distances (e.g., 4 Å) while a small population of ions travel significantly longer distances (e.g., 100 Å) to arrive at the average value of $\lambda_{trap}(T)$. Any distribution of distances traveled is allowable by the ITM as long as the weighted average of distance traveled is $\lambda_{trap}(T)$.

This therefore may suggest a reason for the observed discrepancy between the ITM and NSLR DAE. As we have previously discussed, the NSLR measures all ions, mobile and immobile. It also measures all events that relax the spin energy of the excited mobile cation, even those events that do not take it out of its energy well. However, the dc conductivity experiments only measure those cations that make significant motion out of and away from its energy well. As

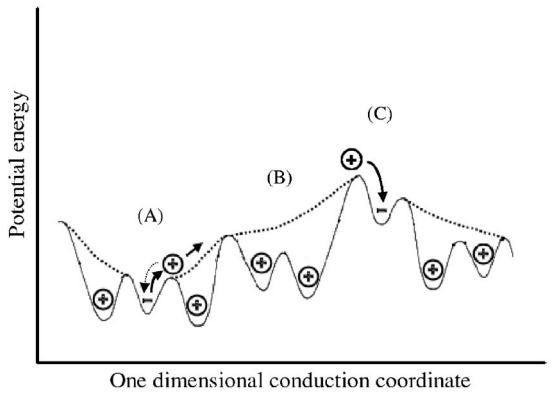

FIG. 14. Possible energy landscape for highly modified FIC glasses showing the effect of filled cation sites on the energies of conducting cations. Cation (A) is first thermally excited as a "free" cation which then has to travel over filled cation sites (B) to find an open cation site (C). As the dashed arrow shows, it can also relax back to its nearby open site. Such backward hops are commonplace in the jump-relaxation models of Funke *et al.*, see for example Refs. 49 and 50.

a result, the dc conductivity is likely to sample a much smaller distribution of the mobile cations, which are in turn likely to explore larger activation energy barriers. This would produce on average a distribution that is narrower and shifted to higher average values, as observed here.

It should be mentioned that the unified site relaxation model developed by Bunde *et al.*[47] suggests a localized hopping back and forth motion until a Coulombic field is relaxed and that the neighboring target site relaxes to adjust for the incoming ion. Our previous neutron scattering measurements for both $Ag_2S+B_2S_3+GeS_2$ (Ref. 48) and $Ag_2S+B_2S_3+SiS_2$ (Ref. 7) glasses have shown that the ion-ion separation is only 3–4 Å for the heavily doped silver glasses. Calculations of the separation distance from the composition and density are also in agreement that the separation distance should be on the order of a few Å. This would also suggest that the cations contributing to the conductivity must travel longer distances to find an open anion site opposed to hopping to the neighboring site, which is already occupied by a cation only a few angstroms away (see Fig. 14).

VI. CONCLUSIONS

This study has shown that the NMR NSLR data of quarternary $LiI+Li_2S+B_2S_3+GeS_2$ glasses can be fitted using weighted sums of the DAE from the binary thioborate and thiogermanate glasses. It has been further determined from the NMR fits that 70%–80% of the lithium ions are associated with the higher on average activation energy germanium sites. No extension or modifications of the DAE model was found necessary to explain the NSLR results over the range of temperature and frequency explored here. On the other hand, while the DAE model provides an excellent fit for the Arrhenius portions of the dc conductivity plots at low temperatures, it is found to fail to predict the non-Arrhenius behavior at higher temperatures. By extending the DAE model to include a temperature-dependent cation conduction distance that arises from a temperature-dependent number of mobile cations, the ITM can be used to accurately fit the dc conductivity at both low (Arrhenius) temperatures and higher (non-Arrhenius) temperatures. It is found, however, that in order to achieve good fits of the dc conductivity over these wide temperature ranges, the ITM uses a DAE width which is one-half to one-third the width of the DAE determined by NSLR measurements. It is suggested that the underlying cause of this discrepancy is that the dc conductivity naturally samples only those mobile cations that can diffuse significant distances, thus experiencing larger energy barriers along the way, whereas the NMR NSLR measurements samples all cations, those in both lower- and higher-energy wells, therefore leading to a broader DAE.

ACKNOWLEDGMENTS

This work was supported in part by the Iowa State University, College of Engineering, the Department of Materials Science and Engineering, the Ames Laboratory of the Department of Energy, and the National Science Foundation under Grant No. NSF-DMR 99-72466. Ames Laboratory is operated for the U.S. Department of Energy by Iowa State University under Grant Contract No. W-7405-Eng-82, supported by the Director for Energy Research, Office of Basic Sciences.

*Present address: Department of Physics, Hunter College, New York, NY 10021, USA.
†Corresponding author.

[1] H. L. Tuller, in *Ceramic Materials for Electronics*, edited by R. C. Buchanan, Materials Engineering series (Marcell Dekker, Inc., New York, 2004), Vol. **25**, p. 87.
[2] K. J. Rao and M. Ganguli, in *Handbook of Solid State Batteries and Capacitors*, edited by M. Z. A. Munshi (World Scientific, Singapore, 1995), pp. 189.
[3] H. L. Tuller, NATO ASI Ser., Ser. B **199**, 51 (1989).
[4] C. A. Angell, Annu. Rev. Phys. Chem. **43**, 693 (1992).
[5] T. Minami, J. Non-Cryst. Solids **73**, 273 (1985).
[6] S. W. Martin, D. M. Martin, J. Schrooten, and B. M. Meyer, J. Phys.: Condens. Matter **15**, S1643 (2003).
[7] J. Schrooten, B. Meyer, and S. W. Martin, J. Non-Cryst. Solids **318**, 27 (2003).
[8] S. W. Martin, J. Schrooten, and B. Meyer, J. Non-Cryst. Solids **307-310**, 981 (2002).
[9] S. W. Martin, F. Borsa, and I. Svare, Proc.-Electrochem. Soc. **2000-32**, 66 (2000).
[10] M. Ribes, G. Taillades, and A. Pradel, Solid State Ionics **105**, 159 (1998).
[11] J. Kincs and S. W. Martin, Phys. Rev. Lett. **76**, 70 (1996).
[12] P. Maass, M. Meyer, A. Bunde, and W. Dieterich, Phys. Rev. Lett.

77, 1528 (1996).
[13] Q. Mei, B. Meyer, D. Martin, and S. W. Martin, Solid State Ionics **168**, 75 (2004).
[14] A. Pradel, N. Kuwata, and M. Ribes, J. Phys.: Condens. Matter **15**, S1561 (2003).
[15] S. W. Martin, J. Am. Ceram. Soc. **74**, 1767 (1991).
[16] M. D. Ingram, Philos. Mag. B **60**, 729 (1989).
[17] A. Pradel and M. Ribes, Mater. Sci. Eng., B **B3**, 45 (1989).
[18] M. D. Ingram, Phys. Chem. Glasses **28**, 215 (1987).
[19] C. T. Moynihan, J. Non-Cryst. Solids **172-174**, 1395 (1994).
[20] S. W. Martin, H. K. Patel, F. Borsa, and D. Torgeson, Solid State Ionics **53-56**, 1141 (1992).
[21] K. L. Ngai, J. N. Mundy, H. Jain, O. Kanert, and G. Balzer-Jollenbeck, Phys. Rev. B **39**, 6169 (1989).
[22] C. Liu and C. A. Angell, J. Non-Cryst. Solids **83**, 162 (1986).
[23] I. Svare, S. W. Martin, and F. Borsa, Phys. Rev. B **61**, 228 (2000).
[24] D. P. Almond, B. Vainas, and N. F. Uvarov, Solid State Ionics **111**, 253 (1998).
[25] K. H. Kim, D. R. Torgeson, F. Borsa, and S. W. Martin, Solid State Ionics **90**, 29 (1996).
[26] K. H. Kim, D. R. Torgeson, F. Borsa, J. Cho, S. W. Martin, and I. Svare, Solid State Ionics **91**, 7 (1996).
[27] T. Akai, S. W. Martin, and F. Borsa, Phys. Rev. B **63**, 024303 (2001).
[28] C. R. Nelson, S. A. Poling, and S. W. Martin, J. Non-Cryst. Solids **337**, 78 (2004).
[29] S. W. Martin and D. R. Bloyer, J. Am. Ceram. Soc. **73**, 3481 (1990).
[30] M. Royle, J. Cho, and S. W. Martin, *Borate Glasses, Crystals and Melts*, Proceedings of the 2nd International Conference on Borate Glasses, Crystals and Melts, Abingdon, UK, 1996 279 (1997).
[31] D. J. Adduci and B. C. Gerstein, Rev. Sci. Instrum. **50**, 1403 (1979).
[32] D. J. Adduci and D. R. Torgeson, Rev. Sci. Instrum. **47**, 1503 (1976).
[33] C. P. Slichter, *Principles of Magnetic Resonance* (Springer-Verlag, New York, 1980), pp. 214ff.
[34] K. L. Ngai, J. Chem. Phys. **98**, 6424 (1993).
[35] M. Tatsumisago, C. A. Angell, and S. W. Martin, J. Chem. Phys. **97**, 6968 (1992).
[36] F. Borsa, D. R. Torgeson, S. W. Martin, and H. K. Patel, Phys. Rev. B **46**, 795 (1992).
[37] N. Bloembergen, E. M. Purcell, and R. V. Pound, Phys. Rev. **73**, 679 (1948).
[38] K. L. Ngai, Solid State Ionics **105**, 225 (1998).
[39] N. F. Mott, Contemp. Phys. **10**, 125 (1969).
[40] N. F. Mott, J. Non-Cryst. Solids **1**, 1 (1968).
[41] M. J. Rice and W. L. Roth, J. Solid State Chem. **4**, 294 (1972).
[42] K. H. Kim, D. R. Torgeson, F. Borsa, J. P. Cho, S. W. Martin, I. Svare, and G. Majer, J. Non-Cryst. Solids **211**, 112 (1997).
[43] K. H. Kim, D. R. Torgeson, F. Borsa, and S. W. Martin, Solid State Ionics **90**, 29 (1996).
[44] B. Meyer, F. Borsa, and S. W. Martin, J. Non-Cryst. Solids **337**, 166 (2004).
[45] Q. Mei, B. Meyer, D. Martin, and S. W. Martin, Solid State Ionics **168**, 75 (2004).
[46] J. A. Schrooten, B. Meyer, and S. W. Martin, Phys. Rev. B (submitted).
[47] A. Bunde, K. Funke, and M. D. Ingram, Solid State Ionics **86-88**, 1311 (1996).
[48] Q. Mei, J. Saienga, J. Schrooten, B. Meyer, and S. W. Martin, Phys. Chem. Glasses **44**, 178 (2003).
[49] K. Funke, R. D. Banhatti, and C. Cramer, Phys. Chem. Chem. Phys. **7**, 157 (2005).
[50] K. Funke, Prog. Solid State Chem. **22**, 111 (1993).